Journal of Advanced Ceramics
2023, **12**(5): 1058–1066
https://doi.org/10.26599/JAC.2023.9220738
ISSN 2226-4108
CN 10-1154/TQ

Research Article

Improving ionic conductivity of von-Alpen-type NASICON ceramic electrolytes via magnesium doping

Il-Seop Jang[a,b,†], Wooseok Go[c,†], Bo-Ye Song[a,b], Hayoung Park[a,b], Yun Chan Kang[b,*], Jinyoung Chun[a,*]

[a]*Emerging Materials R&D Division, Korea Institute of Ceramic Engineering and Technology (KICET), Jinju 52851, Republic of Korea*
[b]*Department of Materials Science and Engineering, Korea University, Seoul 02841, Republic of Korea*
[c]*Energy Storage and Distribution Resources Division, Lawrence Berkeley National Laboratory, Berkeley 94720, USA*

Received: December 22, 2022; Revised: February 9, 2023; Accepted: February 27, 2023

Abstract: NASICON (sodium (Na) superionic conductor) compounds have attracted considerable attention as promising solid electrolyte materials for advanced Na-based batteries. In this study, we investigated the improvement in ionic conductivities of von-Alpen-type NASICON (vA-NASICON) ceramic electrolytes by introducing a magnesium ion (Mg^{2+}) as a heterogeneous element. The optimal Mg-doped vA-NASICON exhibited a high ionic conductivity of 3.64×10^{-3} S·cm^{-1}, which was almost 80% higher than that of un-doped vA-NASICON. The changes in physicochemical properties of the vA-NASICONs through the Mg introduction were systematically analyzed, and their effects on the ionic conductivities of the vA-NASICON were studied in detail. When the optimal ratio of Mg^{2+} was used in a synthetic process, the relative density (96.6%) and grain boundary ionic conductivity (σ_{gb}) were maximized, which improved the total ionic conductivity (σ_t) of the vA-NASICON. However, when Mg^{2+} was introduced in excess, the ionic conductivity decreased because of the formation of an undesired sodium magnesium phosphate ($Na_xMg_yPO_4$) secondary phase. The results of this study are expected to be effectively applied in the development of advanced sodium-based solid electrolytes with high ionic conductivities.

Keywords: NASICON; solid electrolyte; von-Alpen-type; magnesium (Mg) doping; ionic conductivity

1 Introduction

The development of efficient and safe devices for energy storage and utilization is among the most important fields of research in modern society. To this end, in addition to improving established lithium-ion battery technologies, advanced secondary batteries are being actively developed [1–4]. In particular, the research on sodium (Na)-based batteries has increased rapidly since the early 2010s because the raw materials required are inexpensive, abundant, and less-toxic raw materials than those required for other similar batteries [5–7]. In recent years, new types of Na-based batteries based on advanced technologies have been proposed,

† Il-Seop Jang and Wooseok Go contributed equally to this work.
* Corresponding authors.
E-mail: Y. C. Kang, yckang@korea.ac.kr;
J. Chun, jchun@kicet.re.kr

such as all-solid-state Na batteries (ASS-SBs), hybrid sodium–air batteries (HSABs), and seawater batteries (SWBs) [8–11]. A key factor in realizing these new Na-based batteries is the development of solid electrolytes with high ionic conductivity and physicochemical/electrochemical stability [10,12,13].

NASICON (Na superionic conductor)-structured compounds are interesting materials that can be used as solid electrolytes as well as cathodes in secondary batteries [14–21]. Particularly, the NASICON compounds proposed by Hong [22] and Goodenough *et al*. [23], which have the formula of $Na_{1+x}Zr_2Si_xP_{3-x}O_{12}$ ($0 \leqslant x \leqslant 3$), exhibit Na^+ ionic conductivities in the order of 10^{-4} S·cm^{-1} and have wide electrochemical windows; these properties make them suitable for use as the solid electrolytes in the Na-based batteries. Additionally, the NASICON compounds are chemically stable in not only air but also seawater; therefore, they have been adopted as core materials for ceramic electrolytes/separators of secondary SWBs [24,25]. However, the ionic conductivities of the NASICON compounds are relatively low compared to those of general liquid electrolytes (10^{-2} S·cm^{-1}), which causes inferior rate performance of the ASS-SBs and SWBs [26,27]. Therefore, various studies were conducted to improve the ionic conductivities of the NASICON compounds. The introduction of heterogeneous elements is a representative strategy for this purpose [28,29]. The presence of heterogeneous atoms in a bulk crystalline phase of the NASICON compounds can lower the activation energy (E_a) of Na^+ ion transport. Furthermore, the introduction of aliovalent heteroatoms can increase the Na^+ ion ratio in the NASICON compounds for charge compensation, which can lead to an improvement in the ionic conductivities owing to the increased concentration of Na^+ charge carriers [30]. Some heterogeneous elements are known to induce secondary phase formation instead of being incorporated into the bulk phase of the NASICON compounds. Although the ionic conductivity of the secondary phase itself is low, it has been understood that the ionic conductivity of the bulk phase of the NASICONs is improved by the synergistic effect originating from the secondary phase [31,32]. To date, various metal ions, such as La^{3+}, Y^{3+}, Sc^{3+}, Ca^{2+}, magnesium ion (Mg^{2+}), Zn^{2+}, and Ni^{2+}, have been adopted as the heterogeneous elements in the NASICON synthesis process, and the ionic conductivities of the NASICON compounds have been improved via these approaches [27,30–36].

Meanwhile, the NASICON compounds proposed by von Alpen *et al*. [37] and Kuriakose *et al*. [38,39], which have the formula of $Na_{0.8+x}Zr_{1.55}Si_xP_{3-x}O_{11}$, are deficient in ZrO_2. In particular, von-Alpen-type NASICON (vA-NASICON) compounds with a composition of $Na_{3.1}Zr_{1.55}Si_{2.3}P_{0.7}O_{11}$ ($x = 2.3$) exhibited ionic conductivities in the order of magnitude of approximately 10^{-3} S·cm^{-1} [40,41]. This is an improved value compared to the ionic conductivities (~10^{-4} S·cm^{-1}) of Hong-type NASICON (H-NASICON) compounds, represented by the composition $Na_3Zr_2Si_2PO_{12}$. This improvement in the ionic conductivity is considered to be due to a decreased formation of the ZrO_2 secondary phase, which causes a decrease in the ionic conductivities and mechanical strength of the NASICON compounds [40,41]. However, unlike many studies on the H-NASICONs, only a few studies have been conducted on the vA-NASICONs. In addition, there have been few reports on further controlling the composition of the vA-NASICONs and improving their ionic conductivities through the introduction of the heterogeneous elements.

In this study, to address this issue, we investigated the improvement in the ionic conductivities of the vA-NASICON by introducing Mg^{2+} as the heterogeneous element; we adopted Mg^{2+} as the heterogeneous element considering its raw material cost, ionic radius, and oxidation number, as compared with the Zr^{4+} ions present in the NASICON compounds. The changes in physicochemical properties of the vA-NASICONs and the formation of the secondary phase through the Mg introduction were analyzed, and the optimal Mg introduction ratio was confirmed by analyzing the changes in the ionic conductivity. The optimal Mg-doped vA-NASICON showed a high ionic conductivity of 3.64×10^{-3} S·cm^{-1}, which was almost 80% higher than that of the un-doped vA-NASICON, and had a high relative density of 96.6%. The results of this study are expected to be effectively applied for the development and fabrication of the Na-based batteries that require the solid electrolytes with high ionic conductivities.

2 Experimental

2.1 Synthesis of Mg-doped vA-NASICON pellets

Stoichiometric quantities of $Na_3PO_4·12H_2O$ (Sigma-Aldrich, 98.0%), Na_2CO_3 (Sigma-Aldrich, 99.5%),

SiO_2 (Junsei Chemical Co. Ltd.), ZrO_2 (Samchun Chemicals, 99.0%), and MgO (Sigma-Aldrich, 98.0%) were mixed using a planetary milling machine (Pulverisette 7, Fritsch). Na_3PO_4 was used as Na and P precursors, and Na_2CO_3 was used to match the stoichiometry of Na in the Mg-doped vA-NASICON. The mixture was then dried in an oven (J-NDS2, Jisico) at 80 ℃ for 6 h, following which it was calcined at 1100 ℃ for 10 h. Then, the sample was allowed to cool naturally, ground using a planetary milling machine for 6 h, and dried. The resulting calcined powders were compressed into ϕ13 mm pellets and sintered in air at 1250 ℃ for 12 h. The synthesized pellets were polished with silicon carbide abrasive paper until a clean surface appeared. An un-doped sample was prepared for comparison using the same process, but without the addition of MgO.

2. 2 Characterizations of samples

Crystal structures of the sintered samples were studied via an X-ray diffractometer (D8 Advance, Bruker) using Cu Kα radiation (λ = 1.5418 Å) over the diffraction angle (2θ) range of 10°–40°. Microstructural properties of the sample surfaces were investigated using a field-emission scanning electron microscope (FE-SEM; JSM-7610F, JEOL) at an operating voltage of 10.0 kV. Elemental mappings of the samples were performed using an energy-dispersive X-ray spectrometer combined with the FE-SEM. The introduction of Mg was further confirmed by an X-ray photoelectron spectrometer (Nexsa, Thermo Fisher Scientific) with Al Kα radiation (1486.6 eV). The densities of the pellets were measured in deionized (DI) water using Archimedes method, and their relative densities was calculated based on the theoretical density of the NASICON (3.27 $g \cdot cm^{-3}$). For the ionic conductivity measurements, the pellets were prepared by sputtering with Au electrodes on both sides; the thickness of all the pellets was in the range of 1.0–1.2 mm. Electrochemical impedance spectroscopy (EIS) was performed using a potentiostat (SP-300, BioLogic) with a 20 mV amplifier and a frequency range of 1.0 Hz to 7 MHz. Conductivity measurements were performed in a dry room, and Nyquist plots were fitted using the EC-Lab software (Biologic) to obtain the bulk ionic conductivities (σ_b), grain boundary ionic conductivities (σ_{gb}), and total ionic conductivities (σ_t). Temperature dependence of the conductivity was measured at several specific temperatures (T) ranging from 273 to 333 K. Before being tested at each T, the samples were placed at the corresponding T for 1 h. The E_a was calculated by the following equation: $\sigma_t = A/T\exp(-E_a/RT)$, where A is the pre-exponential factor, and R is the gas constant. A Na/electrolyte/stainless steel (SS) cell was used to perform a cyclic voltammetry (CV) curve in the range of −1.0–5.0 V at a scan rate of 1 $mV \cdot s^{-1}$ to determine an electrochemical window of the solid electrolyte. The electronic conductivity was examined by a direct current (DC) polarization experiment at a constant voltage of 3.0 V, and gold was sputtered onto both sides of an electrolyte pellet.

3 Results and discussion

Mg-doped vA-NASICON pellets were prepared using a typical solid-state reaction process (Fig. S1 in the Electronic Supplementary Material (ESM)). All precursors were mixed in a stoichiometric ratio of $Na_{3.1+2x}Zr_{1.55-x}Mg_xSi_{2.3}P_{0.7}O_{11}$ (x = 0, 0.03, 0.05, 0.07, 0.1, 0.15, or 0.2), and the resulting mixture underwent calcination, grinding, pressing, and sintering to fabricate sample pellets. The physicochemical properties of the sample pellets were analyzed after final polishing (Fig. S2 in the ESM). To distinguish each sample, we designated un-doped vA-NASICON ($Na_{3.1}Zr_{1.55}Si_{2.3}P_{0.7}O_{11}$) and Mg-doped vA-NASICON ($Na_{3.1+2x}Zr_{1.55-x}Mg_xSi_{2.3}P_{0.7}O_{11}$) compounds as NZSP and Mg_xNZSP, respectively. In this study, Mg^{2+} ions were adopted as the heterogeneous elements to partially substitute the Zr^{4+} ions in the NZSP; the introduction of aliovalent dopants that substitute Zr^{4+}, e.g., Mg^{2+}, can lead to an increase in the concentration of mobile charge carriers (Na^+) to maintain charge neutrality of the NZSP, thereby improving its ionic conductivity [29]. In addition, because the ionic radius of Mg^{2+} (r_{eff} = 0.72 Å) is the same as that of Zr^{4+}, the distortion in a crystal structure can be minimized [42]. The relatively low cost of the raw materials required compared to those of other dopant candidates, such as Ni^{2+}, Co^{2+}, La^{3+}, Y^{3+}, and Sc^{3+}, is another advantage of Mg^{2+} doping.

Crystalline structures of the NZSP and Mg_xNZSP were analyzed using X-ray diffraction (XRD). The XRD pattern of the NZSP matches well with the NASICON structure with the monoclinic phase (PDF Card No. 01-084-1200) (Fig. 1(a)). Because the

Zr-deficient vA-NASICON composition was targeted in this study, the secondary phase corresponding to ZrO_2, which adversely affects the ionic conductivity of the NASICON, was not observed in the NZSP. The changes in the crystalline structure of the NZSP after the partial substitution of Zr^{4+} with different amounts of Mg^{2+} are shown in Figs. 1(a)–1(d). As the ratio of Mg^{2+} in the Mg_xNZSP increased from 0.03 to 0.1, the peaks at approximately 19.1°, 19.25°, and 30.5° broadened and shifted to higher angles slightly. It is considered that these changes originated from the partial transformation of the monoclinic phase to a rhombohedral phase rather than from the lattice contraction of the NZSP. Similar results were also observed in the study of Sc^{3+}- and Sc^{3+}/Yb^{3+}-doped NASICONs [26]. Such phase transformation was interpreted to be due to the increase in the Na^+ ion concentration, not due to the dopant itself having a similar ionic radius to Zr^{4+}. The presence of Mg^{2+} in the Mg_xNZSP was clearly observed in a Mg 1s X-ray photoelectron spectroscopy (XPS) spectrum (Fig. S3 in the ESM). When the Mg^{2+} dopant ratio was increased to 0.2 ($Mg_{0.2}$NZSP), the NASICON structures were completely transformed to the rhombohedral phase (PDF Card No. 01-084-1575) (Figs. 1(b) and 1(d)). In addition, a large impurity peak corresponding to sodium magnesium phosphate ($Na_xMg_yPO_4$) is observed (Fig. 1(c)).

The ionic conductivities of the NZSP and Mg_xNZSP were analyzed using the EIS measurements at room temperature (25 ℃). Figure 2(a) and Fig. S4 in the ESM show Nyquist plots of each sample, and σ_b, σ_{gb}, and σ_t calculated from the EIS measurements are summarized in Table 1 and Fig. 2(b). The highest ionic conductivity was obtained when Mg^{2+} was introduced at a ratio of 0.05; the $Mg_{0.05}$NZSP exhibited an ionic conductivity of 3.64×10^{-3} S·cm^{-1}, which was almost 80% higher than that of the un-doped NZSP (2.03×10^{-3} S·cm^{-1}) and one of the highest conductivities reported in Refs. [31,33,35,42–44] (Table S1 in the ESM). This can be attributed to a significant decrease in the grain boundary resistance (R_{gb}): MgO, the raw material for the dopant, enhances the densification rate and promotes the grain growth by improving surface diffusion coefficient [42,45,46]. There is no difference between the calcined NZSP and the Mg_xNZSP powders (Fig. S5 in the ESM). However, the SEM image of the polished $Mg_{0.05}$NZSP pellet in a backscattered electron (BSE) mode shows that the $Mg_{0.05}$NZSP has a dense microstructure, and its surface pores are greatly reduced compared to those of the NZSP (Fig. 3(a)). Accordingly, the $Mg_{0.05}$NZSP exhibited a high ionic conductivity

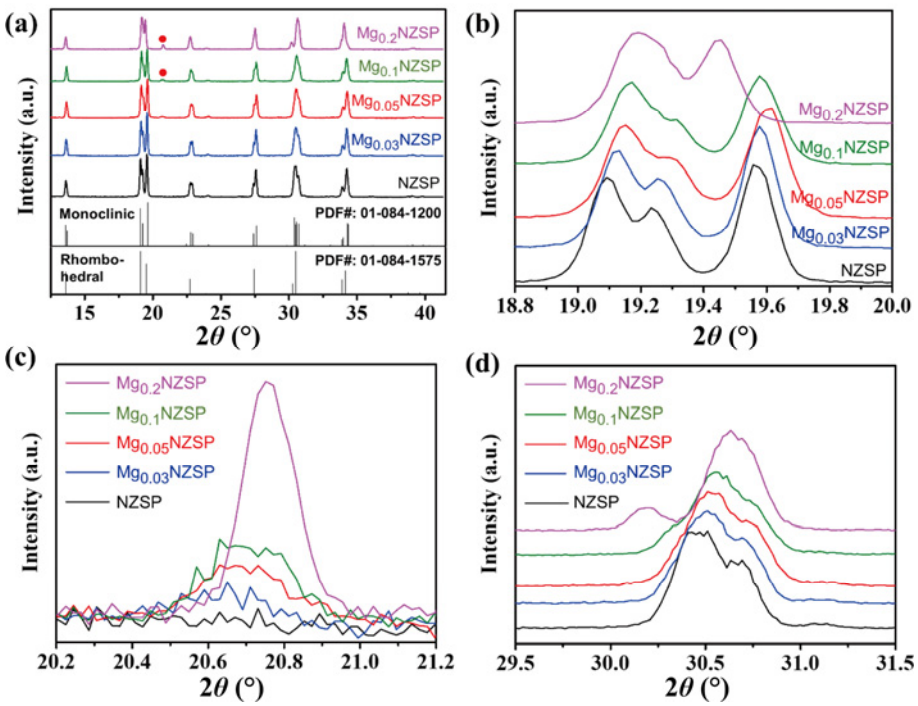

Fig. 1 (a) Overall XRD patterns of NZSP and Mg_xNZSP. The red circles indicate peaks of $Na_xMg_yPO_4$. (b–d) Magnified XRD patterns of selected regions.

based on its high relative density of 96.6% and a significant decrease in R_{gb}. Meanwhile, because the rhombohedral phase has a more symmetric structure than the monoclinic phase, it has a lower E_a for Na^+ diffusion [47,48]. The E_a of the $Mg_{0.05}$NZSP calculated from Arrhenius plot (Fig. 2(d)) was 0.253 eV, which is lower than that of the NZSP (0.266 eV). Therefore, the partial transformation to the rhombohedral phase as well as the increase of the Na^+ concentration can improve σ_b of the NASICON; the increase in σ_b of the $Mg_{0.05}$NZSP is attributed to this reason. The E_a of the $Mg_{0.1}$NZSP increased up to 0.286 eV; it is assumed that E_a increases when the NASICON composition exceeds the optimal range despite its rhombohedral structure. In Ref. [42], the decrease in the ionic conductivities of the NASICON with the transition to the rhombohedral structure was clearly observed when excessive amounts of dopants were used.

However, as the Mg^{2+} ratio increased to 0.07 or more, the ionic conductivity of the Mg_xNZSP decreased compared to that of the $Mg_{0.05}$NZSP; when Mg^{2+} was introduced at a ratio of 0.2, the ionic conductivity of the $Mg_{0.2}$NZSP was less than half that of the un-doped NZSP. Owing to the limited solid solubility of Mg^{2+} in the NASICON compounds, the ionic conductivity reduced when Mg^{2+} was introduced in excess [31,42]: If the Mg^{2+} ratio increased even slightly beyond a certain amount, the secondary phase of $Na_xMg_yPO_4$ with poor ionic conductivity formed, causing the ionic conductivity of the Mg_xNZSP to decrease. The large $Na_xMg_yPO_4$ peak observed in the XRD pattern (Fig. 1(c)) represents the main reason for the low ionic conductivity of the $Mg_{0.2}$NZSP. In addition, wide dark regions were observed throughout the surface in the SEM image of the $Mg_{0.2}$NZSP in the BSE mode (Fig. 3(c)), unlike in that of the $Mg_{0.05}$NZSP. These dark regions arise from the presence of $Na_xMg_yPO_4$, which are composed of lighter elements than those of the Mg_xNZSP, and thus demonstrate the presence of a large number of $Na_xMg_yPO_4$ in the $Mg_{0.2}$NZSP. Unlike the case of using other dopants, e.g., La^{3+} [32], the formation of a $Na_xMg_yPO_4$ secondary phase did not provide a positive effect on σ_b of the NASICON.

The Mg^{2+} distribution and secondary phase formation in the Mg_xNZSP were further confirmed by energy-dispersive X-ray spectroscopy (EDS) mappings (Figs. 3(d) and 3(e)). In the $Mg_{0.05}$NZSP, Mg appeared to be evenly distributed throughout the sample (Fig. 3(d)). In other words, Mg^{2+} was evenly doped into the bulk NASICON phase. In contrast, in the $Mg_{0.2}$NZSP, Mg signals were concentrated in specific regions (Fig. 3(e)). Here, the distribution of Mg overlaps the distribution of P, Na, and O, but is opposite to the distribution of Zr and Si. These results indicate that a large number of $Na_xMg_yPO_4$ secondary phases formed in the $Mg_{0.2}$NZSP.

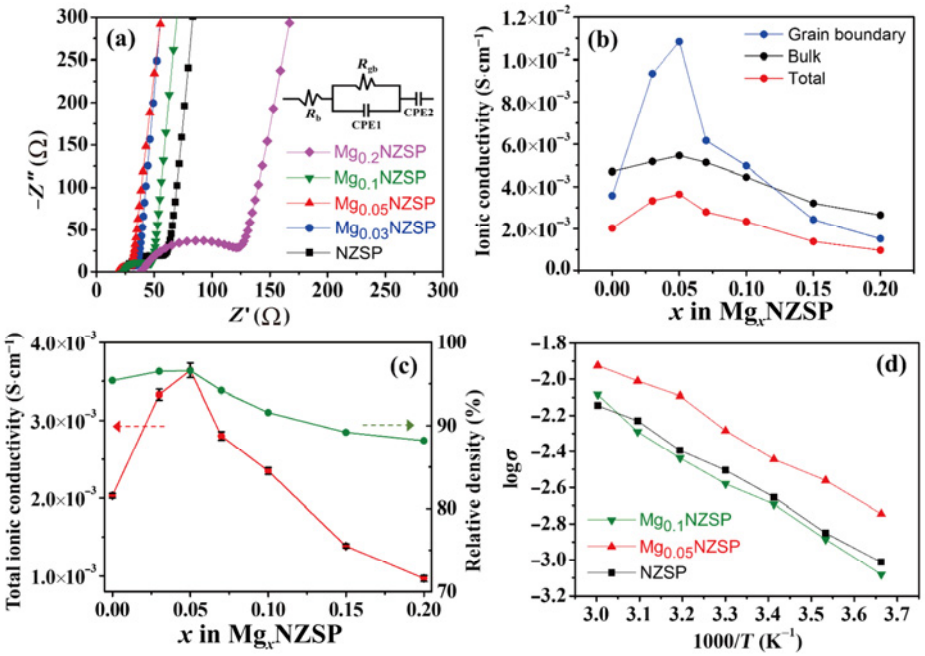

Fig. 2 (a) Nyquist plots, (b) σ_b, σ_{gb}, and σ_t, (c) relative density and σ_t, and (d) Arrhenius plots of NZSP and Mg_xNZSP pellets. Note: R_b is the bulk resistance, and CPE is the abbreviation of the constant phase element.

Table 1 σ_b, σ_{gb}, σ_t, densities, and relative densities of NZSP and Mg_xNZSP

	σ_b ($S\cdot cm^{-1}$)	σ_{gb} ($S\cdot cm^{-1}$)	σ_t ($S\cdot cm^{-1}$)	Density ($g\cdot cm^{-3}$)	Relative density (%)
NZSP	4.71×10^{-3}	3.57×10^{-3}	2.03×10^{-3}	3.121	95.4
$Mg_{0.03}$NZSP	5.17×10^{-3}	9.35×10^{-3}	3.33×10^{-3}	3.155	96.5
$Mg_{0.05}$NZSP	5.46×10^{-3}	1.08×10^{-2}	3.64×10^{-3}	3.160	96.6
$Mg_{0.07}$NZSP	5.13×10^{-3}	6.17×10^{-3}	2.80×10^{-3}	3.080	94.2
$Mg_{0.1}$NZSP	4.45×10^{-3}	4.97×10^{-3}	2.35×10^{-3}	2.997	91.6
$Mg_{0.15}$NZSP	3.22×10^{-3}	2.44×10^{-3}	1.39×10^{-3}	2.916	89.2
$Mg_{0.2}$NZSP	2.66×10^{-3}	1.52×10^{-3}	9.68×10^{-4}	2.885	88.2

The electronic conductivity was analyzed by the DC polarization method. Figure 4(a) shows that the current rapidly approaches 0 A at the applied voltage (3.0 V). The calculated electronic conductivity of the $Mg_{0.05}$NZSP was very low (5.65×10^{-9} $S\cdot cm^{-1}$), and it was slightly lower than that of the NZSP (8.79×10^{-9} $S\cdot cm^{-1}$). The low electronic conductivity and high relative density of the NASICON are effective in suppressing the formation and growth of sodium dendrites [49]. The electrochemical window of the ceramic electrolyte was analyzed through the CV curve in the voltage range of −1.0–5.0 V using the Na/$Mg_{0.05}$NZSP/SS cell. As shown in

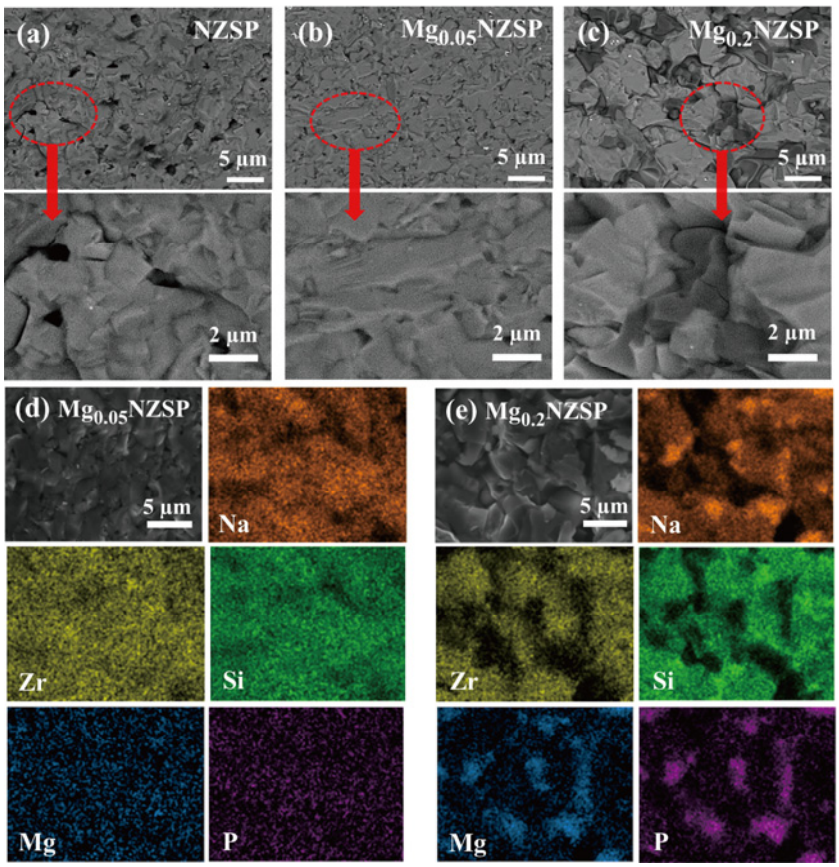

Fig. 3 SEM images of (a) NZSP, (b) $Mg_{0.05}$NZSP, and (c) $Mg_{0.2}$NZSP pellets in BSE mode and elemental mapping results of (d) $Mg_{0.05}$NZSP and (e) $Mg_{0.2}$NZSP pellets.

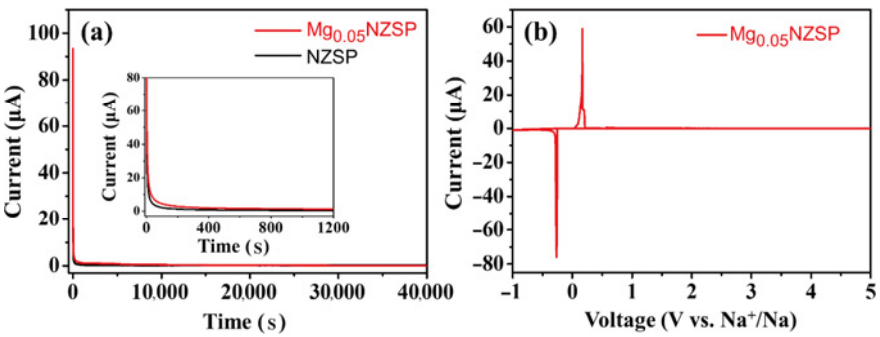

Fig. 4 (a) DC polarization curves of NZSP and $Mg_{0.05}$NZSP. (b) CV curve of $Mg_{0.05}$NZSP.

Fig. 4(b), the $Mg_{0.05}$NZSP has a wide electrochemical window with no oxidation peak at up to 5.0 V. A pair of reversible peaks near 0 V appear owing to reversible Na stripping and plating. Therefore, considering its high ionic conductivity and relative density, low electronic conductivity, and wide electrochemical window, the $Mg_{0.05}$NZSP has ideal properties that make it suitable for sodium–metal-based secondary battery applications.

Summarizing all the results so far, it is important to consider limited solubility of Mg^{2+} in the NASICON when introducing the Mg^{2+} dopant. When the optimal ratio of Mg^{2+} was used in the synthetic process, the relative density and σ_{gb} were maximized so that the Mg_xNZSP with improved properties could be prepared. However, when Mg^{2+} was introduced in excess, the ionic conductivity decreased because of the formation of an undesired $Na_xMg_yPO_4$ secondary phase. Based on the results of this study, it is expected that further research will be conducted in the future to design and manufacture optimal NASICON compositions with higher ionic conductivities and relative density. Furthermore, the chemical stability and mechanical properties of the Mg-doped NASICONs will also be investigated for their practical applications in Na-based secondary batteries.

4 Conclusions

In summary, we developed a highly ion-conductive vA-NASICON ceramic electrolyte via Mg doping. The optimal Mg-doped vA-NASICON ($Mg_{0.05}$NZSP) exhibited a high ionic conductivity of 3.64×10^{-3} S·cm^{-1}, which was almost 80% higher than that of the un-doped vA-NASICON (2.03×10^{-3} S·cm^{-1}), and a high relative density of 96.6%. The transformation of the crystalline structure, the changes in the external surface, and the formation of the secondary phase that were induced by the introduction of the Mg dopant were analyzed, and the effects of these factors on the ionic conductivities of the vA-NASICON were studied. The optimal $Mg_{0.05}$NZSP exhibited a high σ_t based on its high relative density and a significant decrease in R_{gb}. The raw material for the dopant, MgO, could enhance the densification rate and promote grain growth by improving the surface diffusion coefficient. However, when Mg^{2+} was introduced in excess, an undesired secondary phase of $Na_xMg_yPO_4$ with poor ionic conductivity formed, causing the ionic conductivity of the Mg-doped vA-NASICON to decrease. Therefore, it is important to consider the limited solubility of Mg^{2+} in the NASICON when introducing the Mg^{2+} dopant. Based on the results of this study, it is expected that further research will be designed to manufacture the optimal NASICON compositions with higher ionic conductivities.

Acknowledgements

This work was supported by Korea Institute of Energy Technology Evaluation and Planning (KETEP) grant funded by the Korea government (MOTIE) (20215610100040, Development of 20 Wh seawater secondary battery unit cell).

Declaration of competing interest

The authors have no competing interests to declare that are relevant to the content of this article.

Electronic Supplementary Material

Supplementary material is available in the online version of this article at https://doi.org/10.26599/JAC.2023.9220738.

References

[1] Chen RJ, Luo R, Huang YX, *et al*. Advanced high energy density secondary batteries with multi-electron reaction materials. *Adv Sci* 2016, **3**: 1600051.

[2] Lim WG, Kim S, Jo C, *et al*. A comprehensive review of materials with catalytic effects in Li–S batteries: Enhanced redox kinetics. *Angew Chem* 2019, **58**: 18746–18757.

[3] Lim E, Chun J, Jo C, *et al*. Recent advances in the synthesis of mesoporous materials and their application to lithium-ion batteries and hybrid supercapacitors. *Korean J Chem Eng* 2021, **38**: 227–247.

[4] Liu MQ, Wang YH, Wu F, *et al*. Advances in carbon materials for sodium and potassium storage. *Adv Funct Mater* 2022, **32**: 2203117.

[5] Yabuuchi N, Kubota K, Dahbi M, *et al*. Research development on sodium-ion batteries. *Chem Rev* 2014, **114**: 11636–11682.

[6] Vaalma C, Buchholz D, Weil M, *et al*. A cost and resource analysis of sodium-ion batteries. *Nat Rev Mater* 2018, **3**: 18013.

[7] Xu HY, Ruan JH, Liu FL, *et al*. Preparation of lithium-doped NaV_6O_{15} thin film cathodes with high cycling performance in SIBs. *J Korean Ceram Soc* 2022, **59**: 289–301.

[8] Zhao CL, Liu LL, Qi XG, *et al*. Solid-state sodium batteries. *Adv Energy Mater* 2018, **8**: 1703012.
[9] Senthilkumar ST, Go W, Han J, *et al*. Emergence of rechargeable seawater batteries. *J Mater Chem A* 2019, **7**: 22803–22825.
[10] Xu XL, San Hui K, Dinh DA, *et al*. Recent advances in hybrid sodium–air batteries. *Mater Horiz* 2019, **6**: 1306–1335.
[11] Yang HL, Zhang BW, Konstantinov K, *et al*. Progress and challenges for all-solid-state sodium batteries. *Adv Energy Sustain Res* 2021, **2**: 2000057.
[12] Lee C, Wi TU, Go W, *et al*. Unveiling interfacial dynamics and structural degradation of solid electrolytes in a seawater battery system. *J Mater Chem A* 2020, **8**: 21804–21811.
[13] Wu JF, Zhang R, Fu QF, *et al*. Inorganic solid electrolytes for all-solid-state sodium batteries: Fundamentals and strategies for battery optimization. *Adv Funct Mater* 2021, **31**: 2008165.
[14] Jian ZL, Hu YS, Ji XL, *et al*. NASICON-structured materials for energy storage. *Adv Mater* 2017, **29**: 1601925.
[15] Rajagopalan R, Zhang ZN, Tang YG, *et al*. Understanding crystal structures, ion diffusion mechanisms and sodium storage behaviors of NASICON materials. *Energy Storage Mater* 2021, **34**: 171–193.
[16] Yu ZE, Lyu YC, Zou ZY, *et al*. Understanding the structural evolution and storage mechanism of NASICON-structure $Mg_{0.5}Ti_2(PO_4)_3$ for Li-ion and Na-ion batteries. *ACS Sustainable Chem Eng* 2021, **9**: 13414–13423.
[17] Gu ZY, Guo JZ, Sun ZH, *et al*. Air/water/temperature-stable cathode for all-climate sodium-ion batteries. *Cell Rep Phys Sci* 2021, **2**: 100665.
[18] Sun C, Zhao YJ, Ni Q, *et al*. Reversible multielectron redox in NASICON cathode with high energy density for low-temperature sodium-ion batteries. *Energy Storage Mater* 2022, **49**: 291–298.
[19] Yu H, Ruan XP, Wang JJ, *et al*. From solid-solution MXene to Cr-substituted $Na_3V_2(PO_4)_3$: Breaking the symmetry of sodium ions for high-voltage and ultrahigh-rate cathode performance. *ACS Nano* 2022, **16**: 21174–21185.
[20] Wu YC, Meng XH, Yan LJ, *et al*. Vanadium-free NASICON-type electrode materials for sodium-ion batteries. *J Mater Chem A* 2022, **10**: 21816–21837.
[21] Li C, Li R, Liu KN, *et al*. NASICON: A promising solid electrolyte for solid-state sodium batteries. *Interdiscip Mater* 2022, **1**: 396–416.
[22] Hong HYP. Crystal structures and crystal chemistry in the system $Na_{1+x}Zr_2Si_xP_{3-x}O_{12}$. *Mater Res Bull* 1976, **11**: 173–182.
[23] Goodenough JB, Hong HYP, Kafalas JA. Fast Na^+-ion transport in skeleton structures. *Mater Res Bull* 1976, **11**: 203–220.
[24] Jung JI, Kim D, Kim H, *et al*. Progressive assessment on the decomposition reaction of Na superionic conducting ceramics. *ACS Appl Mater Interfaces* 2017, **9**: 304–310.
[25] Hwang SM, Park JS, Kim Y, *et al*. Rechargeable seawater batteries—From concept to applications. *Adv Mater* 2019, **31**: 1804936.
[26] Pal SK, Saha R, Kumar GV, *et al*. Designing high ionic conducting NASICON-type $Na_3Zr_2Si_2PO_{12}$ solid-electrolytes for Na-ion batteries. *J Phys Chem C* 2020, **124**: 9161–9169.
[27] Zhao YJ, Wang CZ, Dai YJ, *et al*. Homogeneous Na^+ transfer dynamic at $Na/Na_3Zr_2Si_2PO_{12}$ interface for all solid-state sodium metal batteries. *Nano Energy* 2021, **88**: 106293.
[28] Rao YB, Bharathi KK, Patro LN. Review on the synthesis and doping strategies in enhancing the Na ion conductivity of $Na_3Zr_2Si_2PO_{12}$ (NASICON) based solid electrolytes. *Solid State Ion* 2021, **366**: 115671.
[29] Yang ZD, Tang B, Xie ZJ, *et al*. NASICON-type $Na_3Zr_2Si_2PO_{12}$ solid-state electrolytes for sodium batteries. *ChemElectroChem* 2021, **8**: 1035–1047.
[30] Jolley AG, Taylor DD, Schreiber NJ, *et al*. Structural investigation of monoclinic–rhombohedral phase transition in $Na_3Zr_2Si_2PO_{12}$ and doped NASICON. *J Am Ceram Soc* 2015, **98**: 2902–2907.
[31] Samiee M, Radhakrishnan B, Rice ZE, *et al*. Divalent-doped $Na_3Zr_2Si_2PO_{12}$ natrium superionic conductor: Improving the ionic conductivity via simultaneously optimizing the phase and chemistry of the primary and secondary phases. *J Power Sources* 2017, **347**: 229–237.
[32] Sun F, Xiang YX, Sun Q, *et al*. Insight into ion diffusion dynamics/mechanisms and electronic structure of highly conductive sodium-rich $Na_{3+x}La_xZr_{2-x}Si_2PO_{12}$ ($0 \leqslant x \leqslant 0.5$) solid-state electrolytes. *ACS Appl Mater Interfaces* 2021, **13**: 13132–13138.
[33] Jolley AG, Cohn G, Hitz GT, *et al*. Improving the ionic conductivity of NASICON through aliovalent cation substitution of $Na_3Zr_2Si_2PO_{12}$. *Ionics* 2015, **21**: 3031–3038.
[34] Ruan YL, Song SD, Liu JJ, *et al*. Improved structural stability and ionic conductivity of $Na_3Zr_2Si_2PO_{12}$ solid electrolyte by rare earth metal substitutions. *Ceram Int* 2017, **43**: 7810–7815.
[35] Chen D, Luo F, Zhou WC, *et al*. Influence of Nb^{5+}, Ti^{4+}, Y^{3+} and Zn^{2+} doped $Na_3Zr_2Si_2PO_{12}$ solid electrolyte on its conductivity. *J Alloys Compd* 2018, **757**: 348–355.
[36] Lu Y, Alonso JA, Yi Q, *et al*. A high-performance monolithic solid-state sodium battery with Ca^{2+} doped $Na_3Zr_2Si_2PO_{12}$ electrolyte. *Adv Energy Mater* 2019, **9**: 1901205.
[37] Von Alpen U, Bell MF, Höfer HH. Compositional dependence of the electrochemical and structural parameters in the NASICON system ($Na_{1+x}Si_xZr_2P_{3-x}O_{12}$). *Solid State Ion* 1981, **3**: 215–218.
[38] Kuriakose AK, Wheat TA, Ahmad A, *et al*. Synthesis, sintering, and microstructure of NASICONs. *J Am Ceram Soc* 1984, **67**: 179–183.
[39] Ahmad A, Wheat TA, Kuriakose AK, *et al*. Dependence of

the properties of NASICONs on their composition and processing. *Solid State Ion* 1987, **24**: 89–97.

[40] Go W, Kim J, Pyo J, *et al*. Investigation on the structure and properties of $Na_{3.1}Zr_{1.55}Si_{2.3}P_{0.7}O_{11}$ as a solid electrolyte and its application in a seawater battery. *ACS Appl Mater Interfaces* 2021, **13**: 52727–52735.

[41] Valle JM, Huang C, Tatke D, *et al*. Characterization of hot-pressed von Alpen type NASICON ceramic electrolytes. *Solid State Ion* 2021, **369**: 115712.

[42] Shen L, Yang J, Liu G, *et al*. High ionic conductivity and dendrite-resistant NASICON solid electrolyte for all-solid-state sodium batteries. *Mater Today Energy* 2021, **20**: 100691.

[43] Sun F, Xiang YX, Sun Q, *et al*. Origin of high ionic conductivity of Sc-doped sodium-rich NASICON solid-state electrolytes. *Adv Funct Mater* 2021, **31**: 2102129.

[44] He SN, Xu YL, Ma XN, *et al*. Mg^{2+}/F^{-} synergy to enhance the ionic conductivity of $Na_3Zr_2Si_2PO_{12}$ solid electrolyte for solid-state sodium batteries. *ChemElectroChem* 2020, **7**: 2087–2094.

[45] Berry KA, Harmer MP. Effect of MgO solute on microstructure development in Al_2O_3. *J Am Ceram Soc* 1986, **69**: 143–149.

[46] Cha JM, Liu LY, Lee HJ, *et al*. Crystallization kinetics of lithium–aluminum–germanium–phosphate glass doped with MgO using a non-isothermal method. *J Korean Ceram Soc* 2021, **58**: 614–622.

[47] Shao YJ, Zhong GM, Lu YX, *et al*. A novel NASICON-based glass–ceramic composite electrolyte with enhanced Na-ion conductivity. *Energy Storage Mater* 2019, **23**: 514–521.

[48] Ran LB, Baktash A, Li M, *et al*. Sc, Ge co-doping NASICON boosts solid-state sodium ion batteries' performance. *Energy Storage Mater* 2021, **40**: 282–291.

[49] Wang XX, Chen JJ, Mao ZY, *et al*. Effective resistance to dendrite growth of NASICON solid electrolyte with lower electronic conductivity. *Chem Eng J* 2022, **427**: 130899.